eNeuro Accepted Manuscript

eNeuro

Research Article: New Research | Disorders of the Nervous System

Loss of retinogeniculate synaptic function in the DBA/2J mouse model of glaucoma

https://doi.org/10.1523/ENEURO.0421-22.2022

Cite as: eNeuro 2022; 10.1523/ENEURO.0421-22.2022

Received: 11 October 2022
Revised: 22 November 2022
Accepted: 8 December 2022

This Early Release article has been peer-reviewed and accepted, but has not been through the composition and copyediting processes. The final version may differ slightly in style or formatting and will contain links to any extended data.

Alerts: Sign up at www.eneuro.org/alerts to receive customized email alerts when the fully formatted version of this article is published.

Copyright © 2022 Smith et al.
This is an open-access article distributed under the terms of the Creative Commons Attribution 4.0 International license, which permits unrestricted use, distribution and reproduction in any medium provided that the original work is properly attributed.

eNeuro Accepted Manuscript

Title: Loss of retinogeniculate synaptic function in the DBA/2J mouse model of glaucoma.

Abbreviated title: Retinogeniculate synapse loss in glaucoma

Authors: Jennie C. Smith[1], Kevin Yang Zhang[1], Asia Sladek[1], Jennifer Thompson[1,2], Elizabeth R. Bierlein[1,2], Ashish Bhandari[1,2], Matthew J. Van Hook[1,3,*]

Author Affiliations: [1]Truhlsen Eye Institute, Department of Ophthalmology & Visual Sciences, University of Nebraska Medical Center, Omaha, NE USA 68198. [2]Department of Pharmacology & Experimental Neuroscience, University of Nebraska Medical Center, Omaha, NE USA 68198. [3]Department of Cellular & Integrative Physiology, University of Nebraska Medical Center, Omaha, NE USA 68198. *Corresponding author

Corresponding Author email address: matt.vanhook@unmc.edu

Number of pages: 35

Number of Figures: 7

Number of tables: 0

Number of words

Abstract: 250

Introduction: 654

Discussion: 1735

Conflict of interest statement: The authors declare that they have no competing interests.

Funding Sources: NIH/NEI R01 grant EY030507 (MJVH), Research to Prevent Blindness/The Glaucoma Foundation Career Advancement Award (MJVH), University of Nebraska Medical Center Graduate

eNeuro Accepted Manuscript

Studies Fellowship (ERB, AB). Funding agencies were not involved in study design, data collection, analysis, interpretation, manuscript preparation, or decision to publish.

Abstract

Retinal ganglion cell (RGC) axons comprise the optic nerve and carry information to the dorsolateral geniculate nucleus (dLGN) which is then relayed to the cortex for conscious vision. Glaucoma is a blinding neurodegenerative disease that commonly results from intraocular pressure (IOP)-associated injury leading to RGC axonal pathology, disruption of RGC outputs to the brain, and eventual apoptotic loss of RGC somata. The consequences of elevated IOP and glaucomatous pathology on RGC signaling to the dLGN are largely unknown yet are likely to contribute to vision loss. Here, we used anatomical and physiological approaches to study the structure and function of retinogeniculate (RG) synapses in male and female DBA/2J (D2) mice with inherited glaucoma before and after IOP elevation. D2 mice showed progressive loss of anterograde optic tract transport to the dLGN and vGlut2 labeling of RGC axon terminals while patch-clamp measurements of RG synaptic function showed that synaptic transmission was reduced in 9 and 12-month D2 mice due to the loss of individual RGC axon inputs. TC neuron dendrites had reduced Sholl complexity at 12 months, suggestive of delayed reorganization following reduced synaptic input. There was no detectable change in RGC density in 11-12m D2 retinas, quantified as the number of ganglion cell layer-residing somata immuno-positive for NeuN and immuno-negative for the amacrine marker choline acetyltransferase (ChAT). Thus, observed synaptic defects appear to precede RGC somatic loss. These findings identify glaucoma- and IOP-associated deficits in an important subcortical RGC projection target, shedding light on processes linking IOP to vision loss.

eNeuro Accepted Manuscript

Significance Statement

Glaucoma is the leading cause of irreversible blindness worldwide and is commonly associated with elevated intraocular pressure (IOP), which triggers loss of retinal ganglion cell (RGC) somata and connections in the retina, axons in the optic nerve, and outputs to visual centers of the brain. We show here that elevated IOP in the DBA/2J mouse model of inherited glaucoma leads to an early-stage and progressive dysfunction of RGC output synapses in the dorsolateral geniculate nucleus (dLGN). As the dLGN is critical for sending signals to the cortex for conscious vision, these findings demonstrate how RGC output synapse loss can contribute to vision loss in glaucoma.

Introduction

Glaucoma is a neurodegenerative disease characterized by sensitivity to intraocular pressure (IOP) and progressive retinal ganglion cell (RGC) degeneration (Calkins, 2012, 2021; Weinreb et al., 2014). The goal of this study was to determine the timing and mechanisms by which IOP leads to loss of RGC output synapses (retinogeniculate/RG synapses) in the mouse dorsolateral geniculate nucleus (dLGN), a subcortical RGC projection target in the thalamus where convergent RGC synaptic inputs to thalamocortical (TC) relay neurons drive TC neuron action potential output to the cortex for conscious vision.

The mechanisms of visual impairment in glaucoma are commonly viewed through the lens of dysfunction progressing toward late-stage apoptotic loss of RGCs. This process occurs as the result of an IOP- and age-induced injury to RGC axons at the optic nerve head (Howell et al., 2007a), where the axons exit the eye, triggering retrograde effects on RGCs and their presynaptic partners in the retina.

eNeuro Accepted Manuscript

However, elevated IOP also alters the function of RGC axons distal to the optic nerve head and at downstream visual targets in the brain, indicating that dysfunction in the RGC projection is likely to contribute to glaucomatous vision loss. These deficits include disruption of optic nerve active transport (Crish et al., 2010), metabolism (Kleesattel et al., 2015; Inman and Harun-Or-Rashid, 2017; Harder et al., 2020; Casson et al., 2021) , and glia (Cooper et al., 2016) as well as alterations to mitochondria (Jassim et al., 2021), RGC excitatory output synapses (Crish et al., 2010; Smith et al., 2016), and the structure and response properties of neurons residing in visual brain nuclei (Bhandari et al., 2019; Van Hook et al., 2020). Evidence to date indicates that many of these functional changes occur early in the pathological process. Evidence from primate and human studies indicates that glaucoma leads to dendritic remodeling and neuronal atrophy within the visual thalamus (Gupta and Yücel, 2003; Gupta et al., 2006, 2007, 2009). In the superior colliculus of DBA/2J mice with inherited glaucoma, ultrastructural studies show that glaucoma leads to atrophy of presynaptic RGC axon terminals, reduced mitochondrial volume, and decreased size of presynaptic active zones (Smith et al., 2016).

The dLGN is an critical subcortical RGC projection target for conscious vision. In rodents, it receives inputs from ~40% of RGCs compared to ~90% of RGCs that project to the superior colliculus (Martin, 1986; Ellis et al., 2016; Seabrook et al., 2017). This contrasts with primates, where RG projections represent a larger proportion of RGC outputs compared to less numerous retinocollicular projections (Perry and Cowey, 1984; Perry et al., 1984). Despite the differences in RG projections between higher- and lower-order mammals (Kerschensteiner and Guido, 2017; Seabrook et al., 2017; Guido, 2018), the rodent dLGN is an accessible system to shed light on the mechanisms of visual system dysfunction in glaucoma. While we have previously probed early-stage changes to RG function in an inducible mouse ocular hypertension model (Bhandari et al., 2019), here we sought to map the timing of functional RG synapse loss and impact of IOP across a wider range of time points in chronic glaucoma. In this study, we therefore made use of the DBA/2J mouse (John et al., 1998; Anderson et al., 2002; Libby

eNeuro Accepted Manuscript

et al., 2005), a commonly used model system that recapitulates many features of human glaucoma. We find that 9-12 month-old DBA/2J mice show IOP-dependent deficits in RGC axonal function, progressive loss of vGlut2-labeled RGC axon terminals, and loss of functional synaptic inputs to each TC neuron. This is accompanied by late-stage reorganization of TC neuron dendrites. Notably, these deficits occurred prior to detectable RGC somatic loss, as assessed using immunofluorescence staining in retinal flat mounts. Thus, we establish the functional consequences of elevated IOP that impair the conveyance of visual signals from RGCs to their post-synaptic targets in the dLGN. The loss of functional RGC output synapses is a major feature of neurodegenerative disease progression and likely to contribute to glaucomatous vision loss.

Materials and Methods

Animals. Animal protocols were approved by the Institutional Animal Care and Use Committee at the University of Nebraska Medical Center. Male and female DBA/2J (D2, Jackson Labs #000671, RRID:IMSR_JAX:000671) and DBA/2J-gpnmb+ (D2-control, Jackson Labs #007048, RRID:IMSR_JAX:007048) (Anderson et al., 2002; Howell et al., 2007b) were bred in-house and housed on a 12h/12h light/dark cycle with standard food and water. Intraocular pressure (IOP) was measured approximately monthly beginning at approximately 2 months of age using an iCare Tonolab rebound tonometer (iCare, Vantaa, Finland) in mice that were lightly anesthetized with isoflurane. Measurements were taken within 3 minutes of isoflurane anesthesia to minimize effects of the anesthesia on IOP. Mice were killed by inhalation of CO_2 followed by cervical dislocation, in keeping with American Veterinary Medical Association guidelines on euthanasia.

Cholera toxin B injections and analysis. To test for deficits in anterograde transport along the optic tract, mice received a unilateral injection of cholera toxin B subunit coupled to Alexa Fluor 594

eNeuro Accepted Manuscript

(CTb-594, Invitrogen C34777). Mice were anesthetized with isoflurane and treated with proparacaine ophthalmic drops (1%). A Hamilton syringe and 33 gauge needle were used to deliver a unilateral intravitreal injection of ~1-2 µL of CTb-594 (1 µg/mL). 3-4 days post-injection, mice were killed with CO_2 asphyxiation and cervical dislocation. Brains were dissected, rinsed briefly in phosphate buffered saline (PBS), and fixed by immersion in 4% paraformaldehyde in PBS overnight. After fixation, brains were rinsed in PBS, cryoprotected overnight in 30% sucrose, embedded in 3% agar, and sliced into 100 micron-thick slices on a Leica VT1000S vibratome. Every other section containing the dLGN was mounted on SuperFrost Plus slides (Fisher Scientific) and coverslipped with Vectashield Hardset (Vector). CTb-594 images of the contralateral dLGN were acquired using a 10x objective lens on an Olympus BX51WI microscope with a Tucsen monochrome camera. To analyze CTb-594 labeling, each image was thresholded in ImageJ based on a region outside of the dLGN and the number of CTb-594 pixels was counted using the histogram. In this way, the total volume of the dLGN labeled by CTb-594 was calculated in serial dLGN sections for each mouse.

Immunofluorescence staining. Retinal ganglion cell axon terminals were labeled by immunofluorescence staining for vGlut2. After euthanasia, brains were dissected into PBS and fixed for 4h in 4% PFA. Brains were then rinsed in PBS, cryoprotected overnight in 30% sucrose, embedded in 3% agar, and cut into 50 micron-thick sections using a Leica VT1000S vibratome. Sections were mounted on SuperFrost Plus slides. For staining, sections were rinsed in PBS, blocked/permeabilized with 0.5% TritonX-100, 5.5% goat serum and 5.5% donkey serum and incubated overnight with a guinea pig polyclonal vGlut2 antibody (1:250, Millipore AB2251-1, RRID:AB_2665454). vGlut2 is a relatively specific marker of RGC axon terminals in the dLGN (Fujiyama et al., 2003; Land et al., 2004; Yoshida et al., 2009; Koch et al., 2011; Seabrook et al., 2013; Bhandari et al., 2022). After primary antibody incubation, slices were rinsed 6x10 minutes and incubated with an AlexaFluor488-conjugated goat-anti-guinea pig IgG (1:200, Invitrogen A-11073, RRID:AB_2534117) for 4 hours, washed 3x5 min in PBS, and coverslipped

eNeuro Accepted Manuscript

137 with Vectashield Hardset. vGlut2 fluorescence was imaged on a Scientifica 2-photon microscope with a
138 MaiTai HP Ti:sapphire laser tuned to 800 nm with a 370x370 micron field of view (2.77 px/micron)
139 centered on the dLGN core. The signal in a single optical section was automatically thresholded and
140 vGlut2 puncta with a size threshold of 6 μm^2 were detected using the Synapse Counter plug-in in ImageJ
141 (Dzyubenko et al., 2016).

142 For measuring retinal ganglion cell density, retinas from D2 and D2-control mice (11-12 months
143 age) were dissected free from the eyecup in Ames solution (US Biologicals, A13722525L). Relieving cuts
144 were made and retinas were mounted on nitrocellulose membranes, after which they were fixed in 4%
145 PFA for 30 mins. After 3x5 minute washes in PBS, retinas were blocked/permeabilized using a solution
146 containing 1% TritonX-100, 5.5% donkey serum, 5.5% goat serum, and 0.5% dimethylsulfoxide for 1
147 hour. Following blocking and permeabilization, retinas were incubated overnight at 4^{o}C in the same
148 solution containing a rabbit-anti-choline acetyltransferase (ChAT) monoclonal antibody (1:1000, Abcam
149 ab178850, RRID:AB_2721842) and a guinea pig-anti-NeuN polyclonal antibody (1:500, Millipore ABN90,
150 RRID:AB_11205592). After 6x10 minutes of washing in PBS, retinas were incubated in AlexaFluor-
151 conjugated secondary antibodies (1:200 goat-anti-guinea pig IgG 568, Invitrogen A-11075,
152 RRID:AB_141954; 1:200 donkey-anti-rabbit IgG-488, Invitrogen A-21206, RRID:AB_2535792) for 4 hours,
153 washed 3x5 mins, mounted on SuperFrost Plus slides and coverslipped with Vectashield Hardset. NeuN
154 and ChAT-labeled cells in the ganglion cell layer were imaged on a 2-photon microscope in 3-4
155 quadrants of the central retina (~500 microns from the optic nerve head) and peripheral retina (~1700
156 microns from the optic nerve head). RGCs counts were performed using an ImageJ macro in which the
157 maximum intensity projections were thresholded, despeckled, and inverted followed by application of
158 the “dilate”, “fill holes”, and “watershed” commands. Finally, the Analyze Particles tool was used to
159 detect objects with a circularity of 0.3-1 with a size threshold of 30 μm^2. Separately, ChAT-labeled
160 amacrine cells were counted with a circularity of 0.4-1 and a size threshold of 80 μm^2. In a subset of

eNeuro Accepted Manuscript

images (n=9), we found that 66% of $ChAT^+$ cells detected using these parameters were also detected as $NeuN^+$. Thus, the RGC number was taken as the difference of NeuN-labeled cells and NeuN/ChAT double-labeled cells, similar to the approach described previously (Buckingham et al., 2008). Density was analyzed separately in central and peripheral retina using the mean cell counts analyzed in this manner from the 3-4 central or peripheral images for each eye.

Patch-clamp electrophysiology. For measurements of retinogeniculate synaptic function, parasagittal sections containing the dLGN (Turner and Salt, 1998; Chen and Regehr, 2000) were prepared using the "protected recovery" method (Ting et al., 2014, 2018) that involved sectioning in an ice-cold artificial cerebrospinal fluid (aCSF; 128 NaCl, 2.5 KCl, 1.25 NaH_2PO_4, 24 $NaHCO_3$, 12.5 glucose, 2 $CaCl_2$, and 2 $MgSO_4$ and continuously bubbled with a mixture of 5% CO_2 and 95% O_2) followed by a 12-minute incubation in an N-methyl-D-glucamine-based solution (in mM: 92 NMDG, 2.5 KCl, 1.25 NaH_2PO_4, 25 glucose, 30 $NaHCO_3$, 20 HEPES, 0.5 $CaCl_2$, 10 $MgSO_4$, 2 thiourea, 5 L-ascorbic acid, and 3 Na-pyruvate, warmed to 33°C). After an additional >1 hour recovery in aCSF at room temperature, slices were transferred to a recording chamber on an Olympus BX51-WI upright microscope and superfused with aCSF supplemented with 60 µM picrotoxin at ~2 mL/minute bubbled with 5% CO_2 and 95% O_2 and warmed to 30-33°C with an in-line solution heater (Warner Instruments).

Thalamocortical (TC) relay neurons were targeted for whole-cell voltage clamp recording based on soma size and morphology using a pipette solution comprised of (in mM) 120 Cs-methanesulfonate, 2 EGTA, 10 HEPES, 8 TEA-Cl, 5 ATP-Mg, 0.5 GTP-Na_2, 5 phosphocreatine-Na_2, 2 QX-314 (pH = 7.4, 300 mOsm). Electrophysiology was performed using a Multiclamp 700B or 700A amplifier, a Digidata 1550B digitizer, and pClamp 10 or 11 software (Axon/Molecular Devices). The holding voltage was -70 mV after correction for the liquid junction potential, which was measured as 10 mV. Series resistance was partially compensated (65-75%) during voltage-clamp recordings of evoked EPSCs, but not during recordings of spontaneous EPSCs (sEPSCs). Signals were sampled at 10 kHz and filtered at 1.6 kHz during

eNeuro Accepted Manuscript

185 acquisition. A concentric bipolar stimulating electrode was positioned in the optic tract anterior and
186 ventral to the ventral LGN (~1-1.5 mm from the dLGN) and used to deliver pairs of current stimuli to RGC
187 axons from an AM Systems Model 2100 Isolated Pulse Stimulator (0.3-0.5 ms, 200 ms inter-stimulus
188 interval).

189 To measure the maximal AMPA receptor-mediated excitatory post-synaptic currents ($EPSC_{AMPA}$),
190 representing the response evoked by all intact RGC inputs converging onto a given TC neuron (Hooks
191 and Chen, 2006, 2008; Litvina and Chen, 2017a), we increased stimulus intensity until the response
192 amplitude plateaued. This was sometimes up to 10 mA stimulus amplitude, which was the maximum of
193 our stimulus generator and only used to ensure the maximum number of inputs were activated; we did
194 not observe signs of damage to the slice after brief use of this stimulus intensity, as we were able to
195 reduce the stimulus amplitude to lower levels and continue to obtain robust responses. NMDA receptor
196 EPSCs ($EPSC_{NMDA}$) were measured as the amplitude 15 ms post-stimulus while the TC neurons were
197 voltage clamped at +40 mV. At this time point, the inward AMPA current had decayed to <4% of its peak
198 amplitude, consistent with prior work measuring $NMDA_{EPSC}$ at RG synapses (Chen and Regehr, 2000; Lin
199 et al., 2014) and indicating this represents a suitable time point for $NMDA_{EPSC}$ measurement. To measure
200 RGC convergence, the stimulus intensity was reduced until it evoked an EPSC representing the input
201 from a single RGC axon (single-fiber EPSC, EPSCsf), defined as the EPSC amplitude recorded when a given
202 stimulus failed to evoke a response approx. 50% of the time. The "fiber fraction" (Hooks and Chen, 2006,
203 2008; Litvina and Chen, 2017a), which is an estimate of the single fiber contribution to the maximal
204 EPSC, and thus, a quantifiable metric for measuring RGC input convergence onto post-synaptic TC
205 neurons, was calculated as the ratio of the EPSCmin/$EPSC_{AMPA}$. These electrophysiology data were
206 analyzed with ClampFit 11.

207 sEPSCs were recorded over sixty seconds in the absence of stimulation and in the presence of 60
208 µM picrotoxin. sEPSCs were detected and amplitude and frequency were analyzed using MiniAnalysis

eNeuro Accepted Manuscript

209 software (Synaptosoft, Fort Lee, NJ, USA) with an amplitude threshold of 4.5 pA. Fits of sEPSC amplitude
210 and baseline noise histograms revealed good separation of sEPSCs from recording noise with these
211 detection parameters. To test whether sEPSCs were dependent on action potential firing in the dLGN
212 slices, after recording control sEPSCs in a handful of slices, they were then were treated with 500 nM
213 tetrodotoxin (Abcam, ab120054) and sPESCs were recorded again.

214 *Single-neuron dye fills and dendritic reconstruction.* For single-neuron dendritic reconstructions,
215 TC neurons in the dLGN core (Krahe et al., 2011) were targeted for whole-cell patch clamp recording in
216 250 micron-thick coronal sections prepared using the protected recovery method, as described above.
217 The pipette solution was either the Cs-methanesulfonate solution, as above, or was a K-gluconate
218 solution (in mM, 120 K-gluconate, 8 KCl, 2 EGTA, 10 HEPES, 5 ATP-Mg, 0.5 GTP-Na_2, 5 Phosphocreatine-
219 Na_2) supplemented with 2% Neurobiotin (Vector Laboratories, SP-1120) and 10 µM CF568 (Biotium).
220 Neurobiotin and CF568 were injected using square-wave current injections (500 pA peak to trough, 2 Hz)
221 for 10-15 minutes in current clamp mode, after which slices were fixed in 4% PFA for 1h and incubated
222 for a week in 10 ug/mL streptavidin-568 in PBS with 1% TritonX-100 at 4^{o}C. After incubation, slices were
223 washed 3x 10 min in PBS, mounted on Superfrost Plus slides and coverslipped with Vectashield Hardset
224 (Vector Laboratories, H-1400). Filled TC neurons were imaged on a 2-photon microscope and dendrites
225 were reconstructed using Simple Neurite Tracer plug-in in ImageJ. Sholl analysis was performed in
226 ImageJ on a 2-dimensional projection of the reconstructed dendrites (10 µm spacing between Sholl
227 rings). Equivalent dendritic field diameter was calculated from the area of a convex polygon drawn by
228 connecting TC neuron dendritic tips in ImageJ.

229 *Experimental design and statistical analyses.* Statistical analysis was performed using GraphPad
230 Prism 9. Normality of the data was assessed using a D'Agostino & Pearson test. When data were
231 normally distributed, significance was assessed using a One-Way Analysis of Variance with Dunnett's

eNeuro Accepted Manuscript

multiple comparison tests. To avoid pitfalls from pseudoreplication (Eisner, 2021), statistical significance was measured using one-way nested ANOVA with a Dunnett's multiple comparisons post-hoc test when we made multiple measurements from single animals (i.e., multiple cells from each mouse in a dataset). Data sets that followed a logarithmic distribution were log transformed prior to statistical testing. For all statistical tests, $p<0.05$ was considered statistically significant. Sample sizes (number of mice and the number of cells), statistical tests, F- or t-statistics, and p-values are reported in the figure legends. For F statistics, we report the between-groups and within-groups degrees of freedom: $F(df_{between}, df_{within})$. We also report the degrees of freedom for the t-statistics: t(df). The IOP integral (mmHg*months, averaging the measurements from both eyes) was measured as the area under the curve of the monthly IOP readings and used to test for a relationship of IOP with measures of dLGN synaptic structure and function. Linear regressions show the best-fit line with 95% confidence bands. Data are displayed as individual data points and mean $\pm$ standard error of the mean (SEM) or median $\pm$ inter-quartile range (IQR), as indicated in figure legends. Control groups represent a mix of D2-control mice from 6-12 months of age, with ages and numbers indicated in the figure legends.

Results

To determine how IOP elevation in DBA/2J mice influences the dLGN, we performed experiments to longitudinally monitor IOP and assess anterograde axoplasmic transport of fluorescently-tagged cholera toxin B (CTb) subunits (Figure 1). D2 mice showed an increase in IOP (n = 168 eyes, 84 mice) beginning at approximately 7 months of age. IOP elevation was variable, as we and others have reported previously (Libby et al., 2005; Inman et al., 2006). Compared to DBA/2J-gpnmb^{+} (D2-control mice, n = 110 eyes, 55 mice), IOP was significantly elevated after 8 months. Notably, IOP in D2 mice was significantly lower than in D2-controls at 5 months and 6 months (Figure 1 B&C), similar to what we

eNeuro Accepted Manuscript

255 have observed previously (Bierlein et al., 2022) and is apparent in figures from other prior studies (Libby
256 et al., 2005; Turner et al., 2017; Rohowetz et al., 2021). While female DBA/2J mice had, on average,
257 higher IOP than males at ages >8 months, consistent with prior work (Libby et al., 2005), the male and
258 female IOP measurements overlapped considerably. Using serial histological sections of the dLGN, we
259 quantified the total fraction of dLGN labeled by anterogradely-transported CTb-594 (Figure 1D-F).
260 Approximately 80% of the dLGN was labeled in D2-control mice, which was similar to the amount
261 labeled in 4 month-old D2 mice and was the result of result of complete labeling from contralateral
262 projections and no labeling in the ipsilateral projection region. By 9 months of age, 29±1% of the dLGN
263 was labeled, and the pattern appeared to be the result of regional loss of transport, similar to what has
264 been documented for the superior colliculus (Crish et al., 2010). There was also a weak but statistically
265 significant correlation of CTb-594 labeling with the IOP integral (Figure 1F), suggesting a functional link
266 between IOP and deficits in anterograde transport to the dLGN.

267 To test for loss of RGC axon terminals, we next immunostained dLGN sections for vGlut2 (Figure
268 2). In these experiments, the density of vGlut2-labeled puncta was comparable between D2-control and
269 4 month-old D2 mice. In older D2 mice, the density of vGlut2-labeled puncta showed a progressive
270 reduction, being lower in 9m and lower still in 12m D2 mice. Of note, we observed very dim vGlut2
271 labeling of presumptive TC neuron somata, which most apparent in sections from 9m and 12m D2 mice
272 with diminished synaptic labeling. This is consistent with prior work indicating that TC neuron axon
273 terminals in the visual cortex express vGlut2 (Nahmani and Erisir, 2005). vGlut2 density in D2 mice was
274 negatively correlated with the IOP integral (Fig 2C). To better understand the relationship between loss
275 of vGlut2 puncta and deficits in anterograde transport to the dLGN, we performed vGlut2
276 immunofluorescence staining on dLGN sections that had also been labeled via anterograde CTb
277 transport (Figure 2D-G). We compared vGlut2 density in regions of 9m D2 dLGN with intact CTb labeling
278 ("CTb-intact") with dLGN regions that had little CTb labeling ("CTb-deficient"). In this experiment, we

eNeuro Accepted Manuscript

found that CTb-deficient regions of the dLGN also had lower vGlut2 puncta density compared to vGlut2 density in the CTb-intact regions. However, this was not a one-to-one relationship; while there was a correlation of CTb labeling intensity with vGlut2 puncta density, regions with very little CTb still had labeling for vGlut2. This result is consistent with findings from the superior colliculus, where anterograde transport loss precedes synaptic loss (Crish et al., 2010; Smith et al., 2016). However, some remaining vGlut2 signal might also originate from tectogeniculate synaptic inputs arising from vGlut2-expressing projection neurons in the stratum griseum superficiale of the superior colliculus (Fremeau et al., 2001; Bickford et al., 2015) or potentially other "replacement terminals" (Whyland et al., 2022).

The above data imply that impaired axonal function (as indicated by reduction in anterograde transport) is related to an impairment of a presynaptic structural marker of RG synapses (vGlut2). Therefore, we next sought to determine the consequences of elevated IOP on RG synaptic function by performing whole-cell voltage-clamp recordings of dLGN TC neurons in a parasagittal slice preparation. First, we recorded spontaneous excitatory post synaptic currents (sEPSCs) in the absence of stimulation and in the presence of 60 mM picrotoxin to block GABAergic inhibition (Figure 3). There was a statistically significant difference in sEPSC frequency between groups. While it was similar in D2-controls and 6m D2 mice, there was a significant reduction in frequency compared to controls at 9m and 12m of age. The Log_{10}(sEPSC frequency) also weakly but significantly correlated with the IOP integral (Figure 3D), pointing to a link between IOP and synaptic dysfunction. We found that sEPSC amplitude (Figure 3E) was not significantly different between groups, suggesting that there was no detectable alteration in AMPA receptor properties or composition at RG synapses. Although these events were recorded in the absence of TTX, they are suitable for estimating quantal parameters in this preparation, as bath application of 500 nM TTX in a separate set of recordings had no effect on either sEPSC frequency or amplitude ($n = 4$, $P>0.05$ paired t-test, Fig 3F), consistent with prior work in guinea pig dLGN (Paulsen and Heggelund, 1996).

eNeuro Accepted Manuscript

303 A reduction in sEPSC frequency here might result from a reduction in the number of functional
304 synapses and/or a reduction in the probability of vesicle release. To probe these possibilities, we used a
305 stimulating electrode positioned in the optic tract to stimulate RGC axons in the presence of 60 µM
306 picrotoxin while we recorded the maximal AMPA receptor-mediated EPSC ($EPSC_{AMPA}$) (Figure 4), which
307 represents the contributions of evoked glutamate release from all intact axons converging onto a given
308 TC neuron. In these experiments, we found that there was a statistically significant difference in
309 $EPSC_{AMPA}$ between groups, with a detectable reduction in $EPSC_{AMPA}$ in slices from 12 month-old D2 mice
310 compared to controls (Figure 4C). The lower $EPSC_{AMPA}$ amplitude was mirrored when we recorded NMDA
311 receptor-mediated EPSCs ($EPSC_{NMDA}$) by changing the holding potential to +40 mV (Figure 4D). There was
312 a weak but statistically significant correlation of $Log_{10}(EPSC_{AMPA})$ with the IOP integral (Figure 4E). There
313 was no significant change in the AMPA/NMDA ratio (Figure 4F) suggesting no changes in the relative
314 contributions of each receptor type at RG synapses or "silent synapses" contributing to the reduced
315 EPSC amplitude. When we measured the responses to a pair of stimuli delivered to the optic tract (200
316 ms inter-stimulus interval), we found that there was a statistically significant difference among the
317 groups, with an increase in the ratio of the second response to the first (Paired pulse ratio/PPR;
318 EPSC2/EPSC1) detectable in 12m D2 mice compared to controls (Figure 4G). In some cases, the PPR was
319 >1 in 12m D2 mice, which represents a shift from the synaptic depression more typical for RG synapses
320 (Turner and Salt, 1998) to a mode of synaptic facilitation, suggestive of a decrease in presynaptic vesicle
321 release probability.

322 We next reduced the stimulus amplitude to evoke synaptic vesicle release from single RGC
323 axons (Figure 5). The ratio of the single fiber EPSC to the maximal EPSC ($EPSCsf/EPSC_{AMPA}$; the "fiber
324 fraction") has been used to monitor the developmental refinement of RGC inputs onto TC neurons and
325 represents a statistically quantifiable estimate of synaptic convergence (Hooks and Chen, 2006, 2008;
326 Litvina and Chen, 2017a). Although there was no significant effect on EPSCsf (Figure 5B), we found that

eNeuro Accepted Manuscript

EPSCsf/$EPSC_{AMPA}$ was significantly increased in 12m D2 mice compared to controls (Figure 5C), indicating a reduction in the number of functional RGC axon inputs onto each TC neuron without substantive change in the contribution from individual RGC axons. The Log_{10}(EPSCsf/$EPSC_{AMPA}$) was weakly, but significantly, correlated with the IOP integral, consistent with a link between eye pressure and loss of RG synapse function in D2 mice (Figure 5D).

Taking the reciprocal of the fiber fraction suggests that each TC neuron receives inputs from an average 6.9 RGC axons in control mice, while 12m D2 mice receive an average of 2.3 functional RGC axon inputs. At the same time point, we detected a reduction in sEPSC frequency by 18 Hz; control sEPSC frequency was 37 Hz while it was 19 Hz in 12m D2 mice. Comparison with published anatomical studies of RG synapses points to the congruence of these two measurements (Morgan et al., 2016; Litvina and Chen, 2017b); if each RGC axon contributes 15 boutons to a post-synaptic TC neuron, each with 27 active zones having a vesicle fusion rate of 0.01 Hz per active zone in the absence of stimulation (Murthy and Stevens, 1999), then the expected result of a drop from 6.9 RGC axonal inputs to 2.3 inputs is an 18 Hz reduction in event frequency. Moreover, for the subset of TC neurons in which we measured both sEPSC frequency and EPSCsf/$EPSC_{AMPA}$, there was a congruence of these two measurements; Log_{10}(sEPSC frequency) was significantly correlated with Log_{10}(EPSCsf/$EPSC_{AMPA}$) (Figure 5 E). This indicates that the change in synaptic transmission measured with both quantal events and optic tract stimulation are of a similar scale and likely to represent complementary measures of a similar pathological process.

The above findings show a loss of vGlut2-labeling of RGC axon terminals and diminished numbers of RGC inputs to each TC neuron in older DBA/2J mice. However, post-synaptic TC neuron structure and function are likely to be altered in glaucoma as well. For instance, elevated IOP is associated with altered TC neuron intrinsic excitability and somatic atrophy (Van Hook et al., 2021). Prior studies have also reported reorganization of LGN neuron dendrites in late-stage glaucoma in primates

eNeuro Accepted Manuscript

(Gupta et al., 2007; Liu et al., 2011; Ly et al., 2011) and we have previously shown changes in TC dendritic structure following bilateral enucleation (Bhandari et al., 2022), a traumatic form of optic nerve injury, and IOP elevation with microbead injections (Bhandari et al., 2019). Here, we performed Sholl analysis of TC neuron dendrites reconstructed after neurobiotin filling during whole-cell recording and found that although TC neuron dendritic complexity was comparable between control and 9m D2 mice, there was a modest reduction in the peak number of Sholl intersections in 12m D2 mice compared to controls (Figure 6). There was no statistically significant difference in equivalent dendritic field diameter among the groups. We also detected a weak but statistically significant correlation of the peak number of Sholl intersections with IOP integral (Figure 6J). Thus, reorganization of post-synaptic TC neuron structure accompanies loss of function of RG synaptic inputs and this is related to IOP.

We next sought to count the number of RGC somata in D2 retinas to provide another comparison of the above findings with a commonly used metric of glaucomatous progression (Figure 7). The use of the neuronal marker NeuN, in conjunction with correction of counts for NeuN-positive cholinergic amacrine cells in the ganglion cell layer (identified by labeling for choline acetyltransferase; ChAT) is a reliable way of counting RGCs and has been used previously to show that somatic loss is a late event in DBA/2J mice (Buckingham et al., 2008; Calkins, 2021). We found that the density of $ChAT^+$ cells in the RGC layer was not significantly different between D2 and D2-control mice (11-12 months age), although it was slightly lower than previously reported in C57Bl/6J and A/J mice, which likely reflects strain differences (Keeley et al., 2007; Whitney et al., 2008). We measured the density of $NeuN^+$ presumptive RGCs by correcting for $ChAT^+/NeuN^+$ double-labeled cells, finding that there was no significant difference in the density of $NeuN^+$ RGCs. This is consistent with and provides confirmation of prior work suggesting that RGC somatic loss is a late event in DBA/2J mice (Buckingham et al., 2008).

eNeuro Accepted Manuscript

Discussion

This study demonstrates a loss of RGC output synapses in the dLGN in a mouse model of glaucoma occurring prior to degeneration of RGC somata. This involves the drop-off of individual RGC inputs to post-synaptic TC neurons without appreciable alterations in the strength of individual RGC inputs. We also find that IOP elevation is associated with diminished anterograde optic tract transport to the dLGN and loss of vGlut2-labeled RGC terminals. These pre-synaptic effects were followed by a modest loss of dendritic complexity in proximal regions of TC neuron dendritic arbors, which might represent a disruption of dendritic homeostasis due to diminished retinogeniculate synaptic inputs. While some results of the current study parallel findings in the superior colliculus in DBA/2J mice and other inducible models of glaucoma (Crish et al., 2010; Chen et al., 2015; Smith et al., 2016), our use of patch clamp electrophysiology studies to probe the functional loss of RGC output synapses in glaucoma is unique and highlights the functional decline of RGC outputs. Although the rodent dLGN receives comparatively fewer RGC inputs than the colliculus, it is an important retinal projection target for conscious vision (Martin, 1986; Ellis et al., 2016; Seabrook et al., 2017). Likewise, its primate equivalent, the LGN, is central to visual function for humans and non-human primates. The rodent dLGN is therefore an approachable system for understanding the impact of eye pressure and glaucomatous degeneration on central visual system function with key relevance for human glaucoma patients (Gupta et al., 2006, 2009).

We used two complementary electrophysiological analyses of dLGN synapses: 1) measurements of sEPSC frequency and 2) evoked RG transmission and fiber fraction measurements. The use of fiber fraction measurements (Hooks and Chen, 2006, 2008; Litvina and Chen, 2017a) showed that TC neurons from 12m D2 mice receive inputs from fewer RGCs than in controls. While the sEPSC results are consistent with several scenarios including loss of synaptic contacts made by each RGC axon or weakening of individual inputs, our data obtained with optic tract stimulation do not indicate a change

eNeuro Accepted Manuscript

in the number of bouton contacts or a major change in the strength of individual synapses, as either process would be reflected in a reduction in the EPSCsf. This instead largely results from drop-off of individual RGC axons, as evidenced by the increase in fiber fraction and no statistically detectable change in single fiber strength. We also observed a change in short-term plasticity, with an increase in the paired-pulse ratio of RG synapses in 12m D2 mice, with some even displaying paired pulse facilitation in contrast to the paired pulse depression typical at these synapses. This change in short-term plasticity likely reflects a reduction in presynaptic vesicle release probability, the origins of which might lie in altered presynaptic calcium dynamics due to compromised mitochondrial health (Smith et al., 2016). Clarifying this will require further study. Notably, using the microbead approach to raise IOP, we have previously found an increase in retinogeniculate vesicle release probability, although we did see a decrease in sEPSC frequency and a similar reduction in TC neuron dendritic complexity (Bhandari et al., 2019), more in line with the current study. The differential effects on release probability are interesting and might reflect differences in mouse age (we used younger mice in the prior study), as older animals have been shown to display more pronounced pathology in response to experimentally-elevated IOP (Crish et al., 2010). Alternatively, the extent and duration of the IOP increase might account for some of the differences, as the microbead model evoked a very modest IOP increase and *ex vivo* experiments were performed only 5 weeks post-bead injection.

vGlut2 labeling studies showed a progressive vGlut2 loss from 9m to 12m. We found that vGlut2 density was related to CTb transport integrity, although a considerable amount of vGlut2 was still present in regions with minimal CTb, suggesting that loss of RGC axon terminal labeling lags transport deficits in the dLGN, although other sources of vGlut2 terminals such as the vGlut2-positive terminals arising from superior colliculus might contribute (Fremeau et al., 2001). It is unknown whether the diminished dLGN vGlut2 labeling in D2 mice reflects degeneration of RGC axon terminals or loss of vGlut2 protein, perhaps due to perturbed transport from the soma. Ultrastructural studies of the D2 SC

eNeuro Accepted Manuscript

show that RGC axon terminals persist in regions deficient for transported CTb (Crish et al., 2010) although they are atrophied and have misshapen mitochondria and smaller active zones (Smith et al., 2016). We did not detect any statistically significant differences in vGlut2 punctum size between transport-intact and -deficient regions at the level of light microscopy. While this might represent a contrast with the RGC axon terminal pathology in the SC (Smith et al., 2016), future ultrastructural studies along with measurements of mitochondrial function will be necessary to test this in the dLGN. We also found that CTb transport to the dLGN was weakly correlated with IOP. Notably, this differs from work in SC, where no such correlation was found (Crish et al., 2010). This might stem from different susceptibility to transport deficits in RGC subpopulations projecting to SC vs dLGN or might instead be reflective of different sensitivity in each study to detect the weak correlation.

In addition to the presynaptic deficits (vGlut2 labeling, CTb transport, and electrophysiological measures), we also show that TC neurons in D2 mice display reorganization of their post-synaptic dendrites. Such dendritic reorganization is a common feature of neurodegenerative diseases (Lin and Koleske, 2010). Prior evidence from primate LGN has identified some dendritic loss in glaucoma (Gupta et al., 2007; Liu et al., 2011; Ly et al., 2011) and we have previously found reductions in TC neuron dendrites in microbead-induced ocular hypertension and following enucleation (Bhandari et al., 2019, 2022). Here, in 12m D2 mice, we find reduced TC neuron dendritic complexity proximal to the soma. This region has a higher concentration of RG inputs compared to the distal dendrites (Robson, 1993; Morgan et al., 2016), where there is a greater concentration of weak corticothalamic feedback synapses. Synaptic inputs are important for dendritic maintenance, with deafferentation or reduced synaptic strength being salient triggers for dendritic loss (Deitch and Rubel, 1989; Flood and Coleman, 1993; Lin and Koleske, 2010). This is a potentially important role of spontaneous synaptic transmission, with spontaneous synaptic input serving a homeostatic function for synaptic maintenance. Retinal input is important for TC neuron dendritic development (El-Danaf et al., 2015; Charalambakis et al., 2019). Thus,

eNeuro Accepted Manuscript

446 it is likely that dendritic loss here is primarily a response to rather than a cause of diminished
447 retinogeniculate synaptic strength. It remains to be tested, however, whether the loss of postsynaptic
448 dendritic complexity is preceded by loss of postsynaptic contacts (i.e. PSD-95 puncta) in D2 TC neurons.
449 Alternatively, portions of the remaining dendritic arbor might lack functional synaptic contacts. This
450 possibility should be explored in future studies. Prior work has also documented several morphological
451 cell classes in mouse dLGN (W-, X-, and Y-cells) with preference for different dLGN regions (Krahe et al.,
452 2011). Our sample focused on the dLGN core region, which is populated mostly by cells with a Y-type
453 radial morphology in healthy animals. It is possible that pathology can complicate identification of cell
454 type by changing dendritic morphology. Additionally, it is unclear whether each cell type will respond to
455 glaucomatous pathology in a similar fashion and this possibility remains to be tested.

456 What is the relationship between dLGN synaptic function and RGC somatic degeneration? Vision
457 impairment in glaucoma is sometimes linked with RGC apoptosis, although numerous degenerative
458 events in somatic/dendritic, axon, and axon terminal "compartments" precede detectable somatic loss
459 (Calkins, 2021). We found no detectable RGC loss in 11-12-month-old D2 mice, which is consistent with
460 prior work showing that RGC somatic loss in D2 mice does not occur until after 15 months of age
461 (Buckingham et al., 2008). RGCs do undergo numerous other structural and functional changes prior to
462 somatic loss in D2 mice including altered dendritic complexity and synapse loss (Della Santina et al.,
463 2013; Williams et al., 2013; Agostinone and Di Polo, 2015; Ou et al., 2016; Risner et al., 2018; Bhandari
464 et al., 2022), intrinsic excitability (Della Santina et al., 2013; Ou et al., 2016; Risner et al., 2018), light
465 responses (Della Santina et al., 2013; Ou et al., 2016; Risner et al., 2018), and metabolic function (Casson
466 et al., 2021; Liu and Prokosch, 2021). Optic nerve pathology including axon expansion, axon loss,
467 reduced neurofilament staining, and astrocyte reorganization are associated with age and IOP and
468 appear to precede RGC somatic loss in DBA/2J mice (Inman et al., 2006; Buckingham et al., 2008; Cooper
469 et al., 2016). Thus, the results of the current study support the body of evidence indicating that

eNeuro Accepted Manuscript

pathological changes to visual system structure and function prior to RGC somatic loss – in this case, diminishment of visual information transfer at the retinogeniculate synapse – contribute to visual impairment in glaucoma.

There are several limitations with the current study and areas for future exploration. First, as discussed above, our results do not differentiate whether glaucoma leads to degenerative loss of synapses, as loss of vGlut2 labeling might result from deficits in axon transport. Moreover, while we show that TC neurons lose dendritic complexity in 12m D2 mice, we do not know whether this is accompanied by a concurrent loss of post-synaptic markers (such as PSD95). Ultrastructural studies of pre- and post-synaptic contacts will be needed to ascertain whether these structures remain intact. Second, differences in dLGN regions receiving input from RGC axons with intact vs. deficient CTb transport might contribute to the variability in measurements of synaptic function we show here. Our data show a relationship between CTb transport integrity and vGlut2 and prior work has shown that transport deficits are related to ultrastructural defects in presynaptic RGC axon terminals in the SC (Crish et al., 2010; Dengler-Crish et al., 2014; Smith et al., 2016). We have not yet explored the link between transport integrity and synaptic function in the dLGN. Third, while we have shown previously that TC neurons are more excitable D2 mice (Van Hook et al., 2020), which might represent a homeostatic maintenance of thalamocortical information transfer following diminished RG synapses, we have not yet explored the consequences of these two phenomena operating in concert; enhanced TC neuron excitability might maintain signaling to the visual cortex until a tipping point in the disease process after which the fidelity of visual signaling is impaired.

eNeuro Accepted Manuscript

493 **References**

494 Agostinone J, Di Polo A (2015) Retinal ganglion cell dendrite pathology and synapse loss: Implications for
495 glaucoma. Prog Brain Res 220:199–216.

496 Anderson MG, Smith RS, Hawes NL, Zabaleta A, Chang B, Wiggs JL, John SWM (2002) Mutations in genes
497 encoding melanosomal proteins cause pigmentary glaucoma in DBA/2J mice. Nat Genet 30:81–
498 85.

499 Bhandari A, Smith JC, Zhang Y, Jensen AA, Reid L, Goeser T, Fan S, Ghate D, Van Hook MJ (2019) Early-
500 Stage Ocular Hypertension Alters Retinal Ganglion Cell Synaptic Transmission in the Visual
501 Thalamus. Front Cell Neurosci 13:426.

502 Bhandari A, Ward TW, Smith J, Van Hook MJ (2022) Structural and Functional Plasticity in the
503 Dorsolateral Geniculate Nucleus of Mice following Bilateral Enucleation. Neuroscience 488:44–
504 59.

505 Bickford ME, Zhou N, Krahe TE, Govindaiah G, Guido W (2015) Retinal and Tectal "Driver-Like" Inputs
506 Converge in the Shell of the Mouse Dorsal Lateral Geniculate Nucleus. J Neurosci 35:10523–
507 10534.

508 Bierlein ER, Smith JC, Van Hook MJ (2022) Mechanism for Altered Dark-Adapted Electroretinogram
509 Responses in DBA/2J Mice Includes Pupil Dilation Deficits. Curr Eye Res 47:897–907.

510 Buckingham BP, Inman DM, Lambert W, Oglesby E, Calkins DJ, Steele MR, Vetter ML, Marsh-Armstrong
511 N, Horner PJ (2008) Progressive ganglion cell degeneration precedes neuronal loss in a mouse
512 model of glaucoma. J Neurosci 28:2735–2744.

eNeuro Accepted Manuscript

513 Calkins DJ (2012) Critical pathogenic events underlying progression of neurodegeneration in glaucoma.
514 Prog Retin Eye Res 31:702–719.

515 Calkins DJ (2021) Adaptive responses to neurodegenerative stress in glaucoma. Prog Retin Eye Res
516 84:100953.

517 Casson RJ, Chidlow G, Crowston JG, Williams PA, Wood JPM (2021) Retinal energy metabolism in health
518 and glaucoma. Prog Retin Eye Res 81:100881.

519 Charalambakis NE, Govindaiah G, Campbell PW, Guido W (2019) Developmental Remodeling of Thalamic
520 Interneurons Requires Retinal Signaling. J Neurosci 39:3856–3866.

521 Chen C, Regehr WG (2000) Developmental remodeling of the retinogeniculate synapse. Neuron 28:955–
522 966.

523 Chen H, Zhao Y, Liu M, Feng L, Puyang Z, Yi J, Liang P, Zhang HF, Cang J, Troy JB, Liu X (2015) Progressive
524 degeneration of retinal and superior collicular functions in mice with sustained ocular
525 hypertension. Invest Ophthalmol Vis Sci 56:1971–1984.

526 Cooper ML, Crish SD, Inman DM, Horner PJ, Calkins DJ (2016) Early astrocyte redistribution in the optic
527 nerve precedes axonopathy in the DBA/2J mouse model of glaucoma. Exp Eye Res 150:22–33.

528 Crish SD, Sappington RM, Inman DM, Horner PJ, Calkins DJ (2010) Distal axonopathy with structural
529 persistence in glaucomatous neurodegeneration. Proc Natl Acad Sci USA 107:5196–5201.

530

531 Deitch JS, Rubel EW (1989) Rapid changes in ultrastructure during deafferentation-induced dendritic
532 atrophy. J Comp Neurol 281:234–258.

eNeuro Accepted Manuscript

533 Della Santina L, Inman DM, Lupien CB, Horner PJ, Wong ROL (2013) Differential progression of structural
534 and functional alterations in distinct retinal ganglion cell types in a mouse model of glaucoma. J
535 Neurosci 33:17444–17457.

536 Dengler-Crish CM, Smith MA, Inman DM, Wilson GN, Young JW, Crish SD (2014) Anterograde transport
537 blockade precedes deficits in retrograde transport in the visual projection of the DBA/2J mouse
538 model of glaucoma. Front Neurosci 8:290.

539 Dzyubenko E, Rozenberg A, Hermann DM, Faissner A (2016) Colocalization of synapse marker proteins
540 evaluated by STED-microscopy reveals patterns of neuronal synapse distribution in vitro. J
541 Neurosci Methods 273:149–159.

542 Eisner DA (2021) Pseudoreplication in physiology: More means less. J Gen Physiol 153:e202012826.

543 El-Danaf RN, Krahe TE, Dilger EK, Bickford ME, Fox MA, Guido W (2015) Developmental remodeling of
544 relay cells in the dorsal lateral geniculate nucleus in the absence of retinal input. Neural Dev
545 10:19.

546 Ellis EM, Gauvain G, Sivyer B, Murphy GJ (2016) Shared and distinct retinal input to the mouse superior
547 colliculus and dorsal lateral geniculate nucleus. J Neurophysiol 116:602–610.

548

549 Flood DG, Coleman PD (1993) Dendritic regression dissociated from neuronal death but associated with
550 partial deafferentation in aging rat supraoptic nucleus. Neurobiol Aging 14:575–587.

551 Fremeau RT, Troyer MD, Pahner I, Nygaard GO, Tran CH, Reimer RJ, Bellocchio EE, Fortin D, Storm-
552 Mathisen J, Edwards RH (2001) The expression of vesicular glutamate transporters defines two
553 classes of excitatory synapse. Neuron 31:247–260.

eNeuro Accepted Manuscript

554 Fujiyama F, Hioki H, Tomioka R, Taki K, Tamamaki N, Nomura S, Okamoto K, Kaneko T (2003) Changes of
555 immunocytochemical localization of vesicular glutamate transporters in the rat visual system
556 after the retinofugal denervation. J Comp Neurol 465:234–249.

557 Guido W (2018) Development, form, and function of the mouse visual thalamus. J Neurophysiol
558 120:211–225.

559 Gupta N, Ang L-C, Noël de Tilly L, Bidaisee L, Yücel YH (2006) Human glaucoma and neural degeneration
560 in intracranial optic nerve, lateral geniculate nucleus, and visual cortex. Br J Ophthalmol 90:674–
561 678.

562 Gupta N, Greenberg G, de Tilly LN, Gray B, Polemidiotis M, Yücel YH (2009) Atrophy of the lateral
563 geniculate nucleus in human glaucoma detected by magnetic resonance imaging. Br J
564 Ophthalmol 93:56–60.

565 Gupta N, Ly T, Zhang Q, Kaufman PL, Weinreb RN, Yücel YH (2007) Chronic ocular hypertension induces
566 dendrite pathology in the lateral geniculate nucleus of the brain. Exp Eye Res 84:176–184.

567 Gupta N, Yücel YH (2003) Brain changes in glaucoma. Eur J Ophthalmol 13 Suppl 3:S32-35.

568 Harder JM, Guymer C, Wood JPM, Daskalaki E, Chidlow G, Zhang C, Balasubramanian R, Cardozo BH,
569 Foxworth NE, Deering KE, Ouellette TB, Montgomery C, Wheelock CE, Casson RJ, Williams PA,
570 John SWM (2020) Disturbed glucose and pyruvate metabolism in glaucoma with
571 neuroprotection by pyruvate or rapamycin. Proc Natl Acad Sci USA 117:33619–33627.

572 Hooks BM, Chen C (2006) Distinct roles for spontaneous and visual activity in remodeling of the
573 retinogeniculate synapse. Neuron 52:281–291.

eNeuro Accepted Manuscript

574 Hooks BM, Chen C (2008) Vision triggers an experience-dependent sensitive period at the
575 retinogeniculate synapse. J Neurosci 28:4807–4817.

576 Howell GR, Libby RT, Jakobs TC, Smith RS, Phalan FC, Barter JW, Barbay JM, Marchant JK, Mahesh N,
577 Porciatti V, Whitmore AV, Masland RH, John SWM (2007a) Axons of retinal ganglion cells are
578 insulted in the optic nerve early in DBA/2J glaucoma. J Cell Biol 179:1523–1537.

579 Howell GR, Libby RT, Marchant JK, Wilson LA, Cosma IM, Smith RS, Anderson MG, John SWM (2007b)
580 Absence of glaucoma in DBA/2J mice homozygous for wild-type versions of Gpnmb and Tyrp1.
581 BMC Genet 8:45.

582 Inman DM, Sappington RM, Horner PJ, Calkins DJ (2006) Quantitative correlation of optic nerve
583 pathology with ocular pressure and corneal thickness in the DBA/2 mouse model of glaucoma.
584 Invest Ophthalmol Vis Sci 47:986–996.

585 Inman DM, Harun-Or-Rashid M (2017) Metabolic Vulnerability in the Neurodegenerative Disease
586 Glaucoma. Front Neurosci 11:146.

587 Jassim AH, Fan Y, Pappenhagen N, Nsiah NY, Inman DM (2021) Oxidative Stress and Hypoxia Modify
588 Mitochondrial Homeostasis During Glaucoma. Antioxid Redox Signal 35:1341–1357.

589 John SW, Smith RS, Savinova OV, Hawes NL, Chang B, Turnbull D, Davisson M, Roderick TH, Heckenlively
590 JR (1998) Essential iris atrophy, pigment dispersion, and glaucoma in DBA/2J mice. Invest
591 Ophthalmol Vis Sci 39:951–962.

592 Keeley PW, Whitney IE, Raven MA, Reese BE (2007) Dendritic spread and functional coverage of
593 starburst amacrine cells. J Comp Neurol 505:539–546.

eNeuro Accepted Manuscript

Kerschensteiner D, Guido W (2017) Organization of the dorsal lateral geniculate nucleus in the mouse. Vis Neurosci 34:E008.

Kleesattel D, Crish SD, Inman DM (2015) Decreased Energy Capacity and Increased Autophagic Activity in Optic Nerve Axons With Defective Anterograde Transport. Invest Ophthalmol Vis Sci 56:8215–8227.

Koch SM, Dela Cruz CG, Hnasko TS, Edwards RH, Huberman AD, Ullian EM (2011) Pathway-specific genetic attenuation of glutamate release alters select features of competition-based visual circuit refinement. Neuron 71:235–242.

Krahe TE, El-Danaf RN, Dilger EK, Henderson SC, Guido W (2011) Morphologically distinct classes of relay cells exhibit regional preferences in the dorsal lateral geniculate nucleus of the mouse. J Neurosci 31:17437–17448.

Land PW, Kyonka E, Shamalla-Hannah L (2004) Vesicular glutamate transporters in the lateral geniculate nucleus: expression of VGLUT2 by retinal terminals. Brain Res 996:251–254.

Libby RT, Anderson MG, Pang I-H, Robinson ZH, Savinova OV, Cosma IM, Snow A, Wilson LA, Smith RS, Clark AF, John SWM (2005) Inherited glaucoma in DBA/2J mice: pertinent disease features for studying the neurodegeneration. Vis Neurosci 22:637–648.

Lin DJ, Kang E, Chen C (2014) Changes in input strength and number are driven by distinct mechanisms at the retinogeniculate synapse. J Neurophysiol 112:942–950.

Lin Y-C, Koleske AJ (2010) Mechanisms of synapse and dendrite maintenance and their disruption in psychiatric and neurodegenerative disorders. Annu Rev Neurosci 33:349–378.

eNeuro Accepted Manuscript

614 Litvina EY, Chen C (2017a) Functional Convergence at the Retinogeniculate Synapse. Neuron 96:330-
615 338.e5.

616 Litvina EY, Chen C (2017b) An evolving view of retinogeniculate transmission. Vis Neurosci 34:E013.

617 Liu H, Prokosch V (2021) Energy Metabolism in the Inner Retina in Health and Glaucoma. IJMS 22:3689.

618 Liu M, Duggan J, Salt TE, Cordeiro MF (2011) Dendritic changes in visual pathways in glaucoma and other
619 neurodegenerative conditions. Exp Eye Res 92:244–250.

620 Ly T, Gupta N, Weinreb RN, Kaufman PL, Yücel YH (2011) Dendrite plasticity in the lateral geniculate
621 nucleus in primate glaucoma. Vision Res 51:243–250.

622 Martin PR (1986) The projection of different retinal ganglion cell classes to the dorsal lateral geniculate
623 nucleus in the hooded rat. Exp Brain Res 62:77–88.

624 Morgan JL, Berger DR, Wetzel AW, Lichtman JW (2016) The Fuzzy Logic of Network Connectivity in
625 Mouse Visual Thalamus. Cell 165:192–206.

626 Murthy VN, Stevens CF (1999) Reversal of synaptic vesicle docking at central synapses. Nat Neurosci
627 2:503–507.

628 Nahmani M, Erisir A (2005) VGluT2 immunochemistry identifies thalamocortical terminals in layer 4 of
629 adult and developing visual cortex. J Comp Neurol 484:458–473.

630

631 Ou Y, Jo RE, Ullian EM, Wong ROL, Della Santina L (2016) Selective Vulnerability of Specific Retinal
632 Ganglion Cell Types and Synapses after Transient Ocular Hypertension. J Neurosci 36:9240–
633 9252.

eNeuro Accepted Manuscript

634 Paulsen O, Heggelund P (1996) Quantal properties of spontaneous EPSCs in neurones of the guinea-pig
635 dorsal lateral geniculate nucleus. J Physiol 496 (Pt 3):759–772.

636 Perry VH, Cowey A (1984) Retinal ganglion cells that project to the superior colliculus and pretectum in
637 the macaque monkey. Neuroscience 12:1125–1137.

638 Perry VH, Oehler R, Cowey A (1984) Retinal ganglion cells that project to the dorsal lateral geniculate
639 nucleus in the macaque monkey. Neuroscience 12:1101–1123.

640 Risner ML, Pasini S, Cooper ML, Lambert WS, Calkins DJ (2018) Axogenic mechanism enhances retinal
641 ganglion cell excitability during early progression in glaucoma. Proc Natl Acad Sci USA
642 115:E2393–E2402.

643 Robson JA (1993) Qualitative and quantitative analyses of the patterns of retinal input to neurons in the
644 dorsal lateral geniculate nucleus of the cat. J Comp Neurol 334:324–336.

645 Rohowetz LJ, Mardelli ME, Duncan RS, Riordan SM, Koulen P (2021) The Contribution of Anterior
646 Segment Abnormalities to Changes in Intraocular Pressure in the DBA/2J Mouse Model of
647 Glaucoma: DBA/2J-Gpnmb +/SjJ Mice as Critical Controls. Front Neurosci 15:801184.

648 Seabrook TA, El-Danaf RN, Krahe TE, Fox MA, Guido W (2013) Retinal input regulates the timing of
649 corticogeniculate innervation. J Neurosci 33:10085–10097.

650 Seabrook TA, Burbridge TJ, Crair MC, Huberman AD (2017) Architecture, Function, and Assembly of the
651 Mouse Visual System. Annu Rev Neurosci 40:499–538.

652 Smith MA, Xia CZ, Dengler-Crish CM, Fening KM, Inman DM, Schofield BR, Crish SD (2016) Persistence of
653 intact retinal ganglion cell terminals after axonal transport loss in the DBA/2J mouse model of
654 glaucoma. J Comp Neurol 524:3503–3517.

eNeuro Accepted Manuscript

655 Ting JT, Daigle TL, Chen Q, Feng G (2014) Acute brain slice methods for adult and aging animals:
656 application of targeted patch clamp analysis and optogenetics. Methods Mol Biol 1183:221–242.

657 Ting JT, Lee BR, Chong P, Soler-Llavina G, Cobbs C, Koch C, Zeng H, Lein E (2018) Preparation of Acute
658 Brain Slices Using an Optimized N-Methyl-D-glucamine Protective Recovery Method. J Vis Exp.

659 Turner AJ, Vander Wall R, Gupta V, Klistorner A, Graham SL (2017) DBA/2J mouse model for
660 experimental glaucoma: pitfalls and problems. Clin Experiment Ophthalmol 45:911–922.

661 Turner JP, Salt TE (1998) Characterization of sensory and corticothalamic excitatory inputs to rat
662 thalamocortical neurones in vitro. J Physiol (Lond) 510 (Pt 3):829–843.

663 Van Hook MJ, Monaco C, Bierlein ER, Smith JC (2020) Neuronal and Synaptic Plasticity in the Visual
664 Thalamus in Mouse Models of Glaucoma. Front Cell Neurosci 14:626056.

665 Weinreb RN, Aung T, Medeiros FA (2014) The pathophysiology and treatment of glaucoma: a review.
666 JAMA 311:1901–1911.

667 Whitney IE, Keeley PW, Raven MA, Reese BE (2008) Spatial patterning of cholinergic amacrine cells in
668 the mouse retina. J Comp Neurol 508:1–12.

669 Whyland KL, Hernandez Y, Slusarczyk AS, Guido W, Bickford ME (2022) The parabigeminal nucleus is a
670 source of “retinogeniculate replacement terminals” in mice that lack retinofugal input. J Comp
671 Neurol.

672 Williams PA, Howell GR, Barbay JM, Braine CE, Sousa GL, John SWM, Morgan JE (2013) Retinal ganglion
673 cell dendritic atrophy in DBA/2J glaucoma. PLoS ONE 8:e72282.

eNeuro Accepted Manuscript

674 Yoshida M, Satoh T, Nakamura KC, Kaneko T, Hata Y (2009) Cortical activity regulates corticothalamic
675 synapses in dorsal lateral geniculate nucleus of rats. Neurosci Res 64:118–127.

676

677

678 **Figure Legends**

679 **Figure 1 – Elevated intraocular pressure and deficits in anterograde transport to the dLGN. A)**
680 Intraocular pressure (IOP) measurements from DBA/2J-gpnmb+ (D2-control) mice (n = 110 eyes from 55
681 mice included in this study). **B)** IOP measurements from DBA/2J (D2) mice (n = 168 eyes from 84 mice).
682 **C)** Mean (± SEM) IOP measurements from D2 and D2-control eyes. Unpaired t-tests: 2m (month)
683 $t(147)=2.942$, $p=0.0038$; 3m $t(205)=1.539$, $p=0.13$; 4m $t(183)=0.275$, $p=0.78$; 5m $t(203)=6.883$, $p=1.0\times10^{-10}$; 6m $t(163)=8.992$, $p=2.3\times10^{-14}$; 7m $t(143)=1.47$, $p=0.14$; 8m $t(155)=6.144$, $p=6.6\times10^{-9}$; 9m $t(119)=7.29$, $p=4.0\times10^{-11}$; 10m $t(81)=6.881$, $p=1.3\times10^{-9}$; 11m $t(69)=4.63$, $p=2.5\times10^{-5}$. **D)** Fluorescently-tagged cholera
686 toxin-B (CTb) was injected unilaterally in to the vitreous and the area of labeled contralateral dLGN was
687 measured based on fluorescence signal in serial dLGN sections. **E)** Group data (mean ± SEM) showing
688 fraction of CTb-labeled dLGN. There was a significant difference among groups (one-way ANOVA,
689 $F(3,28)=15.0$, $p=5.2\times10^{-6}$) and the 9m group significantly differed from the control group (Dunnett's
690 multiple comparison test; $p<1\times10^{-15}$). **F)** For the D2 mice, there was a significant negative correlation
691 (linear regression with 95% confidence interval) of the fraction of dLGN labeled by CTb with the IOP
692 integral (Pearson correlation, $F(1,16)=15.22$, $p=0.0013$). Sample size: Control n = 14 (controls by age: 4m
693 = n 4, 6m n = 6, 9m n = 4); 4m D2 N = 5; 6m D2 n = 6; 9m D2 n = 7.

694

695 **Figure 2 – Loss of vGlut2 labeled RGC axon terminals in the dLGN is associated with transport deficits**
696 **in DBA/2J mice. A)** Single optical sections of dLGN labeled with an anti-vGlut2 antibody from a D2-

eNeuro Accepted Manuscript

control mouse and D2 mice at 4m, 9m, and 12m of age. Zoomed-in images with detected puncta from the 4m and 12m D2 images are shown to the right. **B)** Group data (mean ± SEM) showing density of detected vGlut2 puncta. There was a significant difference among groups (one-way ANOVA, $F(3,35)=12.87$; $p=8.0\times10^{-6}$) with 9m and 12m groups differing significantly from the control group (Dunnett's multiple comparison: 4m p=0.98; 9m p=0.0070; 12m $p<1\times10^{-15}$). **C)** vGlut2 density was significantly correlated with IOP integral ($F(1,24)=23.11$; p=0.000068). **D)** Analysis of vGlut2 density in regions of the dLGN with intact or deficient anterograde transport of unilaterally-injected CTb. D2-control mice total n = 13 (D2-control by age: 4m n = 6; 9m n = 5; 12m = 2); 4m D2 n = 4; 9m D2 n = 11; 12m D2 n = 11. **E)** Quantification (mean ± SEM) of CTb pixel intensity in "intact" or "deficient" dLGN regions ($t(5)=4.489$, p=0.0065, paired t-test). **F)** Quantification of vGlut2 density (mean±SEM) in dLGN regions with intact or deficient CTb labeling ($t(5)=2.743$, p=0.041, paired t-test, n = 6 D2 mice). **G)** Significant positive correlation (linear regression with 95% confidence interval) of vGlut2 density with intensity of CTb labeling (Pearson correlation, $F(1,10)=9.812$, p=0.011).

Figure 3 – Progressive loss of miniature excitatory post-synaptic currents recorded from dLGN thalamocortical relay neurons in DBA/2J mice. **A)** Recording schematic of optic tract (OT), ventral lateral geniculate nucleus (vLGN), and dLGN with patch clamp electrode in parasagittal slice. **B)** Left: Example 5-second duration traces of spontaneous quantal excitatory post-synaptic currents (sEPSCs) recorded in the without stimulation from D2-control and D2 mice. Right: average of the detected sEPSC waveforms. **C)** Group data (median ± IQR) of sEPSC frequency. There was a significant difference among groups (nested one-way ANOVA, $F(3,33)=6.038$, p=0.0021) and 9-month and 12-month groups differed significantly from control (Dunnett's multiple comparison: 6m p=0.99; 9m p=0.026; 12m p=0.0078). **D)** There was a weak but significant correlation of Log10(sEPSC frequency) measured in TC neurons from D2 mice with the IOP integral ($F(1,79)=17.2$; p=0.000084). **E)** Group data (median ± IQR) of sEPSC

eNeuro Accepted Manuscript

amplitude. There was no significant difference among groups (nested one-way ANOVA, $F(3,34)=1.696$, $p=0.19$) and individual groups were not significantly different from the control (Dunnett's multiple comparison, 6m $p=0.24$; 9m $p=0.29$; 12m $p=0.21$). Group sizes: D2 control total n=48 cells, 13 mice (D2-control by age: 6m n = 11 cells, 3 mice; 9m n = 27 cells, 8 mice; 12m n = 10 cells, 2 mice). 6m D2 n=28 cells, 7 mice; 9m D2 n=20 cells, 8 mice; 12m D2 n=33 cells, 10 mice. **F)** Group data (mean ± SEM) of sEPSC amplitude and frequency recorded before and after bath application of 500 nM tetrodotoxin (TTX, n = 4 TC neuron recordings). TTX did not have a significant effect on either amplitude ($t(3)=2.020$, $p=0.137$, paired t-test) or frequency ($t(3)=0.014$, $p=0.99$, paired t-test).

Figure 4 – Retinogeniculate inputs to TC neurons in D2 mice. **A)** Recording schematic of optic tract (OT) with stimulating electrode, ventral lateral geniculate nucleus (vLGN), and dLGN with patch clamp electrode in parasagittal slice. **B)** Example maximal AMPA- and NMDA-receptor-mediated EPSCs recorded at -70 mV and +40 mV, respectively, following maximal stimulation of the optic tract with a pair of pulses (200 ms inter-stimulus-interval). **C)** Group data of the AMPA-receptor-mediated maximal EPSC ($EPSC_{AMPA}$) shows that the EPSC differed among the groups (nested one-way ANOVA, $F(3,36)=11.23$, $p= 2.4\times10^{-5}$). The $EPSC_{AMPA}$ was significantly smaller in amplitude in recordings from 12m D2 mice compared to controls (Dunnett's multiple comparison test: 6m $p=0.77$; 9m $p=0.16$; 12m $p<1\times10^{-15}$). **D)** The NMDA-receptor-mediated EPSC differed among groups (nested one-way ANOVA, $F(3,38)=10.51$, $p=3.6\times10^{-5}$) and the 12m amplitudes were significantly lower than control (Dunnett's multiple comparison: 6m $p=0.97$; 9m $p=0.54$; 12m $p<1\times10^{-15}$). **E)** There was a weak but statistically significant correlation of $Log_{10}(EPSC_{AMPA})$ with the IOP integral ($F(1,70)=24.5$, $R^2 = 0.26$, $p=0.0000049$). **F)** The AMPA/NMDA ratio did not significantly differ across groups (nested one-way ANOVA, $F(3,38)=1.145$, $p=0.34$). Group sizes: control total n = 46 cells, 16 mice (controls by age 6m n = 18 cells, 5 mice; 9m n = 23 cells, 9 mice; 12m n = 5 cells, 2 mice). **G)** Paired pulse ratio differed among groups (nested one-way

eNeuro Accepted Manuscript

745 ANOVA, F(3,38)=6.608, p=0.0011) and was significantly higher in 12m D2 mice compared to controls
746 (Dunnett's multiple comparison: 6m p=0.75; 9m p=0.79; 12m p=0.0040). C, D, F, and G) Show median ±
747 IQR. Sample sizes: Control, n=40 cells, 12 mice (controls by age: 6m n=13 cells, 4 mice; 9m n = 22 cells, 8
748 mice; 12m n = 5 cells, 2 mice); 6m n=21 cells, 7 mice; 9m n=21 cells, 9 mice; 12m n=29-31 cells, 10 mice.

749 **Figure 5 – Progressive loss of convergent retinal inputs to dLGN relay neurons in DBA/2J mice. A)**
750 Example maximal EPSCs ($EPSC_{AMPA}$) and single-fiber EPSCs (EPSCsf) from a control and 12m D2 mouse. **B)**
751 The single-fiber EPSC amplitude (median ± IQR) did not differ among groups (nested one-way ANOVA,
752 F(3,35)=1.445, p=0.25). **C)** The "fiber fraction" ($EPSCsf/EPSC_{AMPA}$; median ± IQR) significantly differed
753 among groups (nested one-way ANOVA, F(3,35)=4.604, p=0.0081) and the 12m value was significantly
754 different from control (Dunnett's multiple comparison; 6m p=0.71, 9m p=0.10; 12m p=0.0033). **D)** The
755 $Log_{10}(EPSCsf/EPSC_{AMPA})$ weakly but significantly correlated with the IOP integral in D2 mice (F(1,65)=7.15
756 R^2=0.099, p=0.0095). Sample sizes: Control, n=40 cells, 12 mice (controls by age: 6m n=13 cells, 4 mice;
757 9m n = 22 cells, 8 mice; 12m n = 5 cells, 2 mice); 6m n=21 cells, 7 mice; 9m n=21 cells, 9 mice; 12m n=26
758 cells, 9 mice. **E)** Log_{10}(sEPSC frequency) weakly but significantly correlated with $Log_{10}(EPSCsf/EPSC_{AMPA})$
759 (F(1,53)=7.99, R^2=0.13, p=0.0066). 6m n = 18 cells, 7 mice; 9m n = 14 cells, 7 mice; 12m n = 23 cells, 9
760 mice.

761

762 **Figure 6 – Thalamocortical neuron dendritic remodeling in DBA/2J mice. A-C)** Top row: Maximum
763 intensity projections of filled TC neurons filled with Neurobiotin during whole-cell recording in coronal
764 slices from control (A), 9m D2 (B), and 12m D2 (C) mice. Bottom row: TC neuron dendrite
765 reconstructions. **D-F)** Sholl plots of each TC neuron included in the sample. **G)** Group data (mean ± SEM)
766 of Sholl plots. **H)** Group data (mean ± SEM) of the peak number of Sholl intersections for each cell. There
767 was a significant difference among groups (nested one-way ANOVA, F(2,16)=8.346, p=0.0033) and the

eNeuro Accepted Manuscript

12m peak intersections was significantly lower than control (Dunnett's multiple comparison, 9m p=0.46; 12m p=0.0019). **I)** Group data (mean ± SEM) of the dendritic field diameter measured as the equivalent diameter of a convex polygon of the dendritic field. There was no statistically significant difference among groups (nested one-way ANOVA, $F(2,16)=0.2320$, $p=0.80$). **J)** There was a weak but statistically significant correlation of the peak number of Sholl intersections with the IOP integral for mice with complete IOP records ($F(1,18)=5.65$, $R^2=0.24$, $p=0.029$). Sample size: Control n = 15 cells (8 D2-control mice ages 4m-12m); 9m-10m D2 n=15 cells (7 mice); 12m D2, n=8 cells (5 mice).

Figure 7 – No loss of retinal ganglion cell somata in 11-12-month-old DBA/2J mice. A) 2-photon Immunofluorescence images of retinal flat mounts from a 12-month-old D2-control mouse and a 12 month-old D2 mouse stained with antibodies for NeuN and choline acetyl transferase (ChAT). Images were acquired from central retina (centered ~500 microns from the optic nerve head) and peripheral retina (centered ~1700 microns from the optic nerve head). **B)** Analysis of $ChAT^+$ cell density (median ± IQR). Each data point is the $ChAT^+$ cell density averaged across three to four quadrants for each retina. There was no significant difference in $ChAT^+$ cell density between D2-control and D2 mice (central $t(15)=0.7860$, $p=0.44$; peripheral $t(15)=0.8289$, $p=0.42$, unpaired t-test). **C)** RGC density was measured as the difference between the total number of $NeuN^+$ cells and the number of $NeuN^+/ChAT^+$ double-labeled cells. There was no significant difference between D2-control and D2 RGC density (central $t(15)=0.4230$, $p=0.68$; peripheral $t(15)=0.0920$, $p=0.93$, unpaired t-test). Sample sizes: D2-control, n=8 retinas, 4 mice; D2, n=9 retinas, 5 mice.

eNeuro Accepted Manuscript

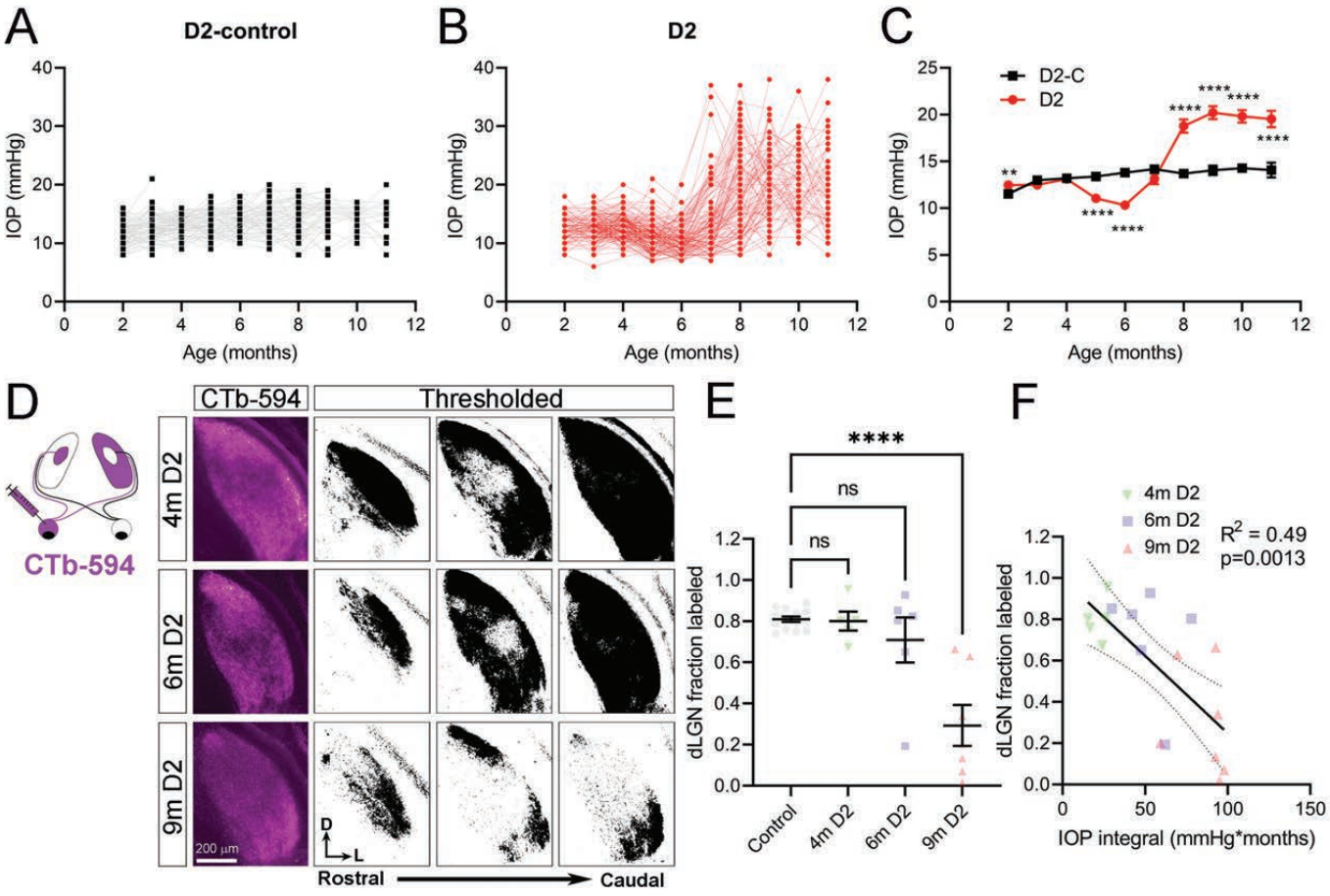

eNeuro Accepted Manuscript

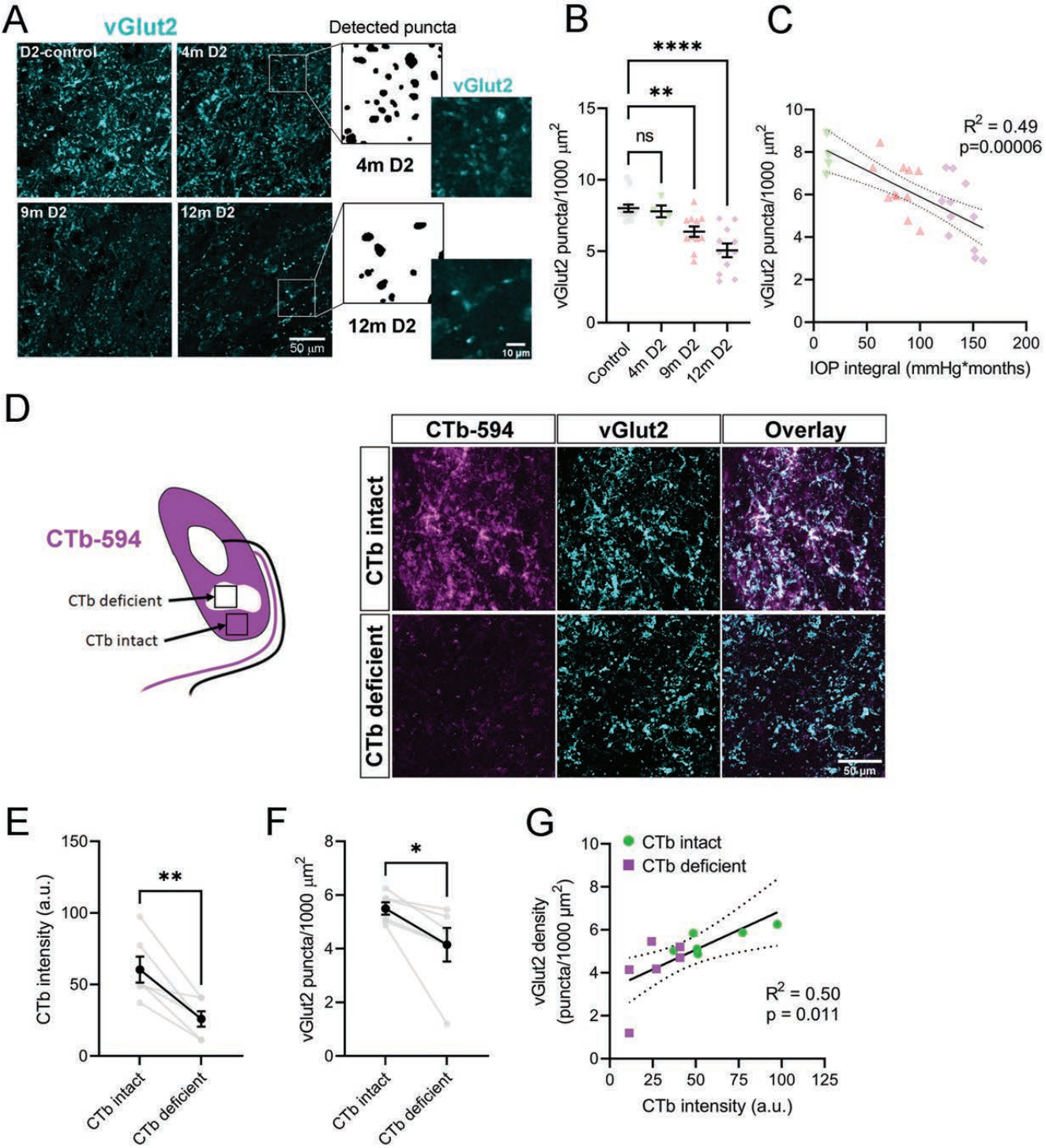

eNeuro Accepted Manuscript

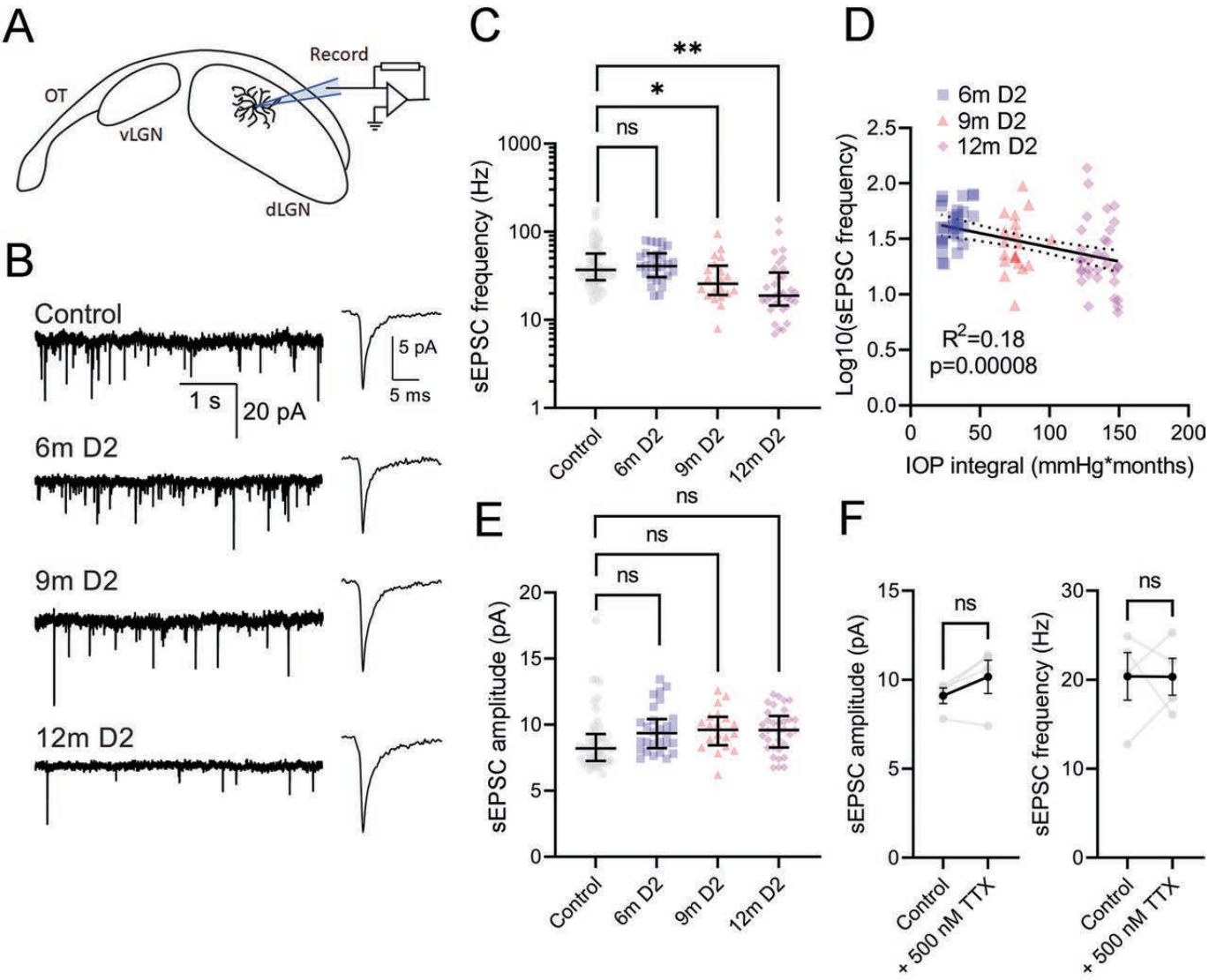

eNeuro Accepted Manuscript

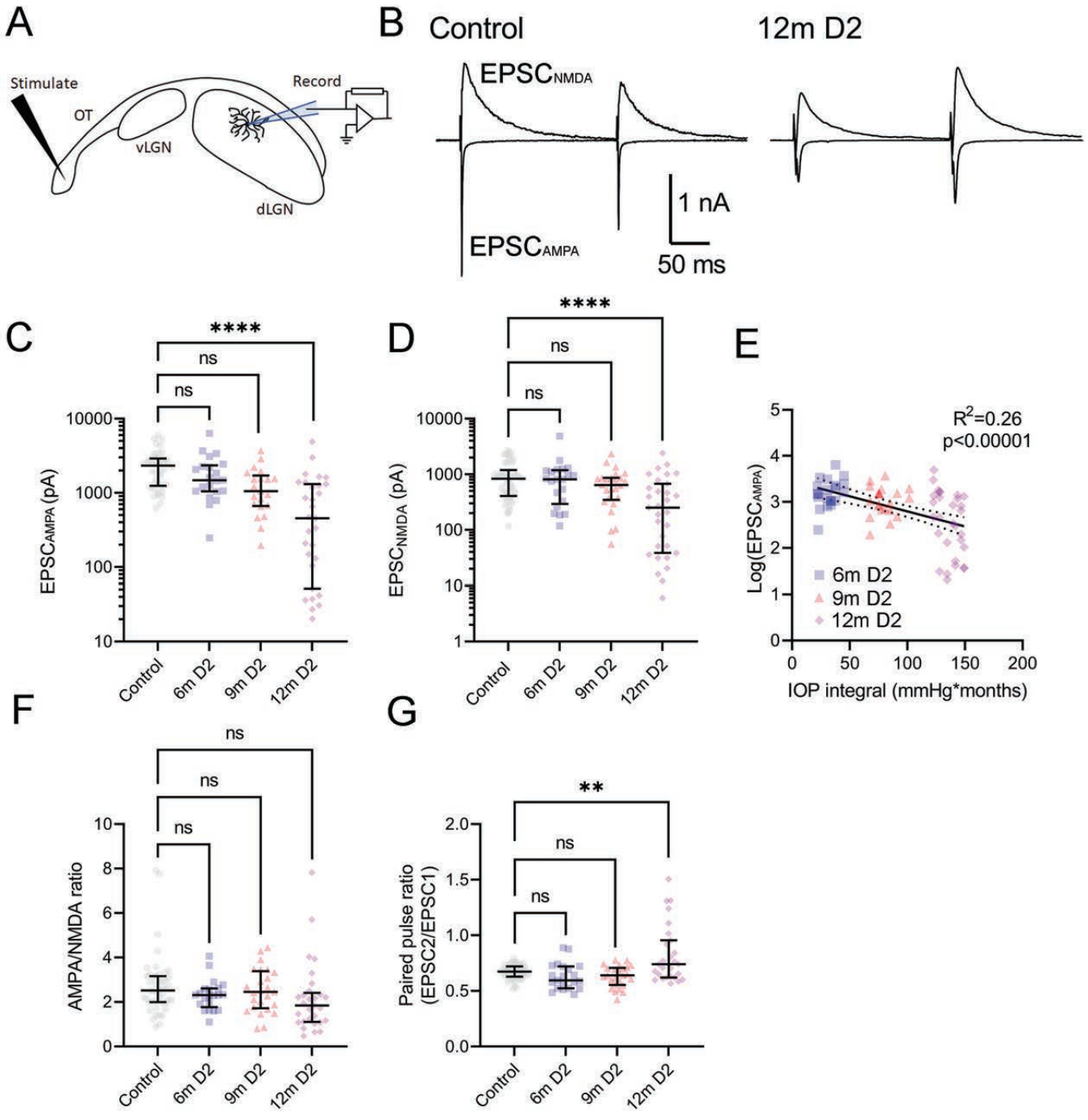

eNeuro Accepted Manuscript

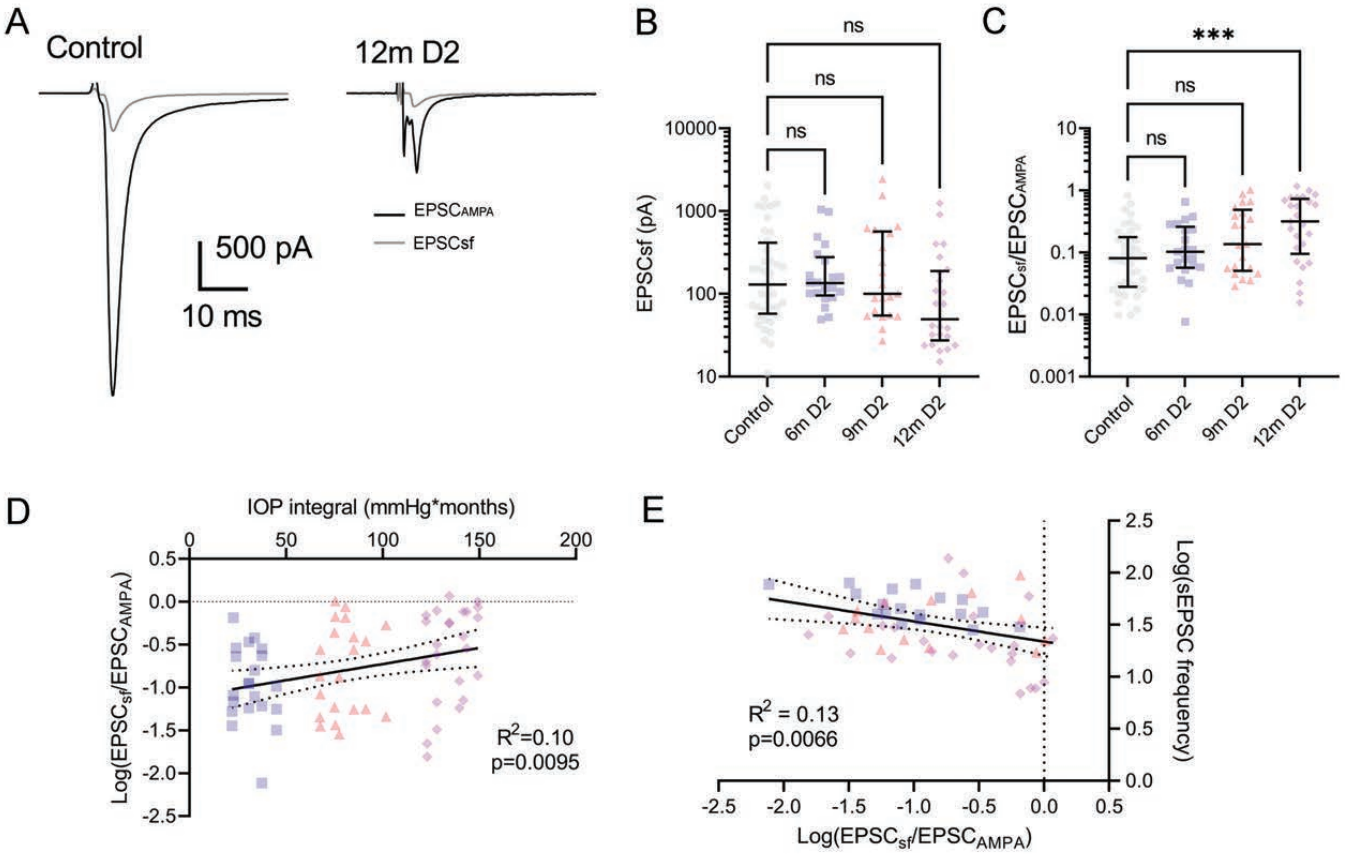

eNeuro Accepted Manuscript

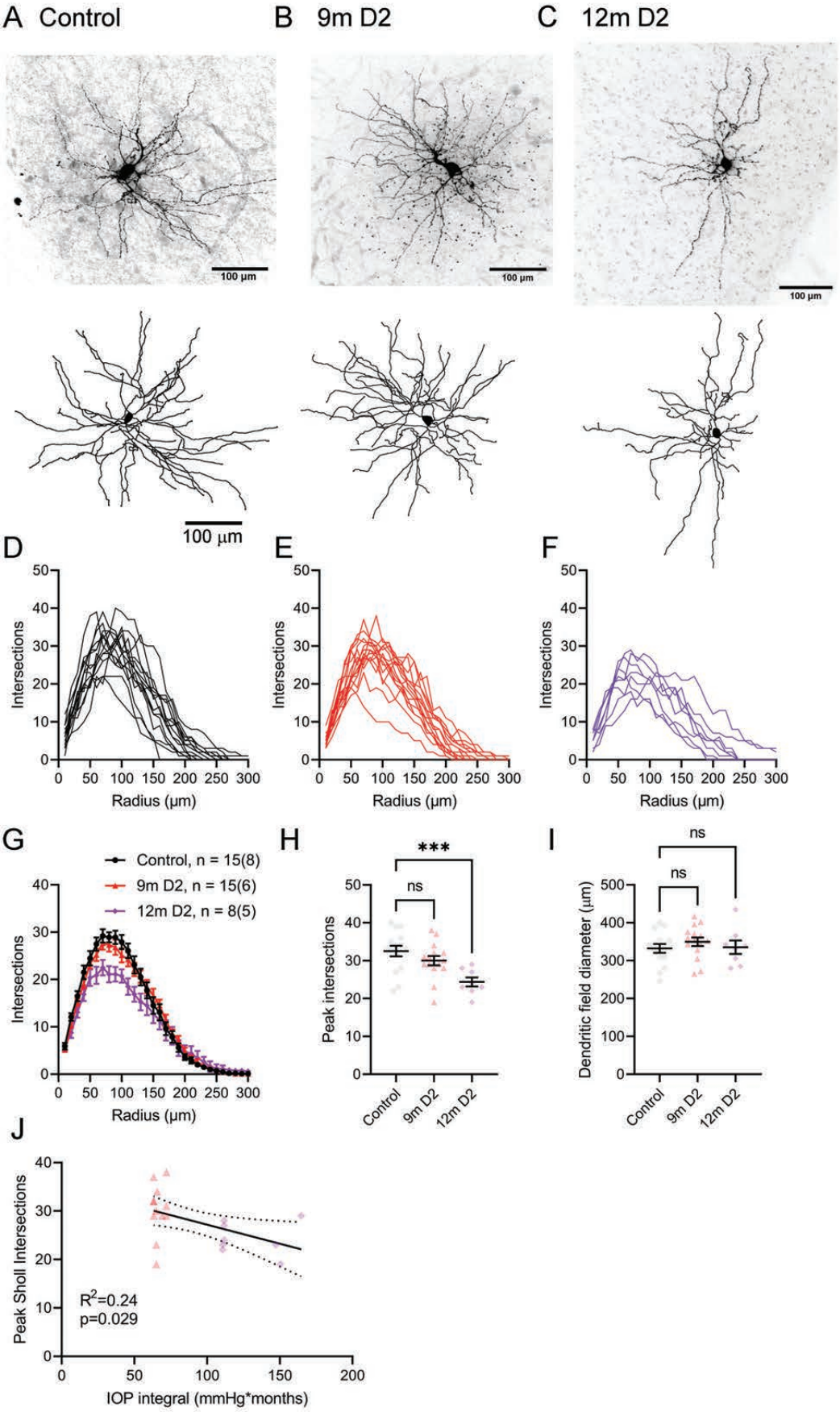
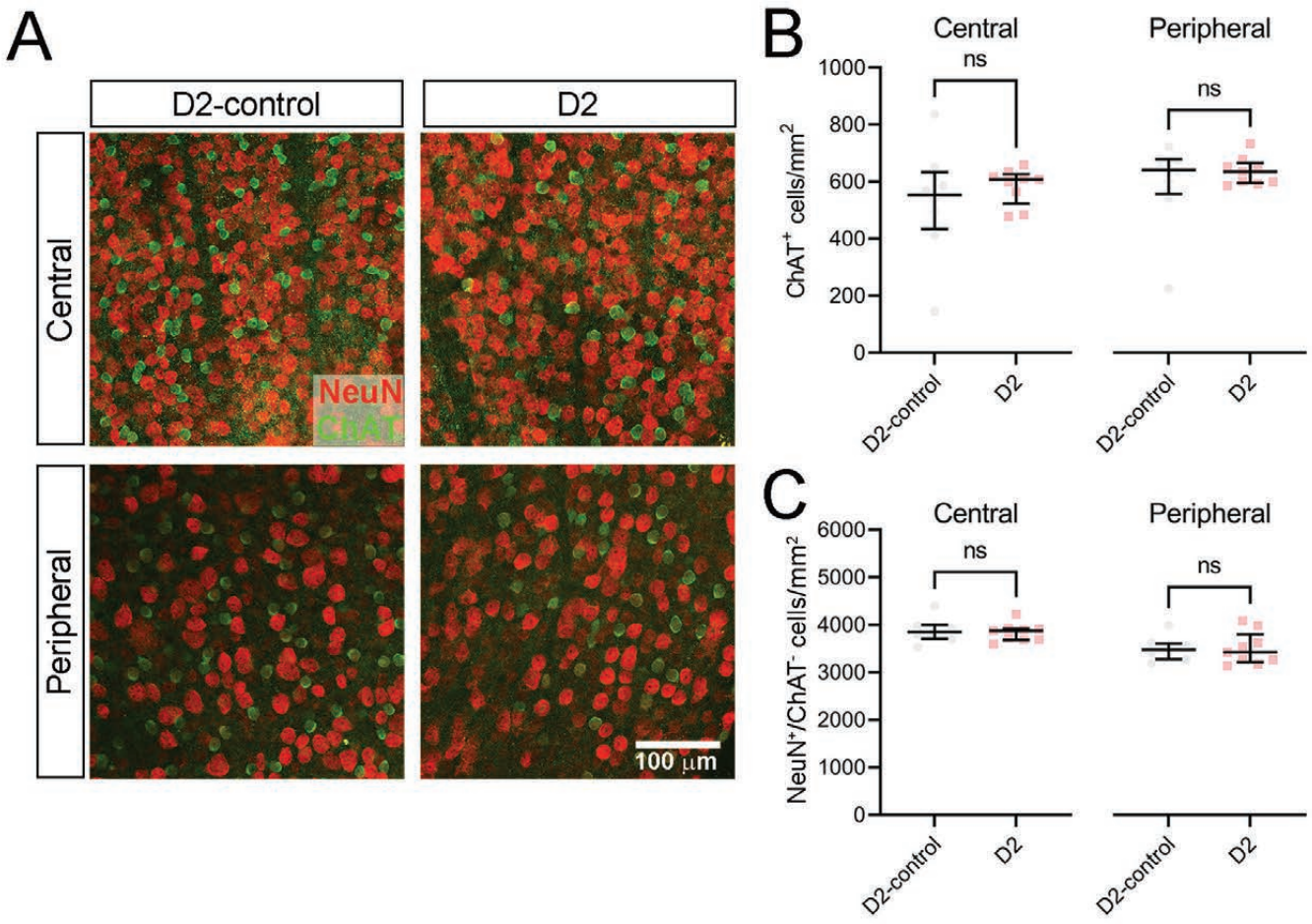
eNeuro Accepted Manuscript